Poloidally resolved measurements of the perpendicular propagation velocity of density fluctuations in ASDEX Upgrade L-mode plasmas

To cite this article: K Höfler *et al* 2021 *Plasma Phys. Control. Fusion* **63** 035020

OPEN ACCESS
IOP Publishing
Plasma Physics and Controlled Fusion
Plasma Phys. Control. Fusion **63** (2021) 035020 (10pp)
https://doi.org/10.1088/1361-6587/abd896

Poloidally resolved measurements of the perpendicular propagation velocity of density fluctuations in ASDEX Upgrade L-mode plasmas

K Höfler[1,2], T Happel[2], P Hennequin[3], U Stroth[1,2], M Cavedon[2], R Dux[2], R Fischer[2], R M McDermott[2], E Poli[2], C U Schuster[1,2], E Wolfrum[2] and the ASDEX Upgrade Team[4]

[1] Physik Department E28, Technische Universität München, 85748 Garching, Germany
[2] Max Planck Institut für Plasma Physik, 85748 Garching, Germany
[3] Laboratoire de Physique des Plasmas, CNRS, Ecole Polytechnique, 91128 Palaiseau, France

E-mail: klara.hoefler@ipp.mpg.de

Received 31 July 2020, revised 9 December 2020
Accepted for publication 5 January 2021
Published 20 January 2021

Abstract

Poloidal asymmetries of the propagation velocity of density fluctuations perpendicular to the magnetic field measured with Doppler reflectometry have been reported in several magnetic confinement plasma devices. Careful analysis of a large variety of different low confinement mode plasma scenarios performed at the ASDEX Upgrade tokamak does not reveal such an asymmetry outside the uncertainties of the evaluation process of the measurement data. The perpendicular velocity is investigated between mid-radius and the plasma edge and follows the poloidal dependence of the $E \times B$ drift velocity regardless of the probed turbulence structure size. Compared to measurements of a charge exchange recombination spectroscopy diagnostic this points towards a significantly smaller phase velocity than the $E \times B$ drift velocity. The analysis technique is presented in a representative discharge together with a sensitivity study of the impact of density, magneto hydrodynamic equilibrium and diagnostic alignment on the interpretation of the measured Doppler shift using ray tracing and thus on poloidal asymmetries. Three more highly different plasma scenarios with poloidally symmetric velocity profiles are shown.

Keywords: perpendicular velocity, phase velocity, plasma flows, plasma turbulence, Doppler reflectometry, tokamak

(Some figures may appear in colour only in the online journal)

1. Introduction

Magnetic confinement fusion power plants will have high energy confinement times, plasma densities and temperatures. These parameters are directly influenced by turbulence which is the main player to cause transport of heat and particles in a tokamak [1, 2]. Plasma turbulence is decorrelated and dissipated by sheared plasma flows. The latter are believed to play a crucial role in the reduction of turbulence and the development of a pedestal in the transition from the low to the high plasma confinement mode [3]. Because of the above, they are an important input parameter for modelling turbulence or transport and consolidated experimental observations are of major interest.

Various diagnostic techniques such as Doppler reflectometry (DR) and charge exchange recombination spectroscopy

[4] See author list of H Meyer *et al* 2019 *Nucl. Fusion* **59** 112014.

(CXRS) allow to evaluate plasma flows in the confined region experimentally and make them accessible for comparison to simulations. Poloidal asymmetries of the perpendicular velocity have been reported on the TEXTOR tokamak [4] using correlation reflectometry and on the Tore Supra tokamak [5] and the TJ-II heliac [6], both using DR. The term *perpendicular* refers to the direction perpendicular to both the confining magnetic field and the normal to the flux surfaces. While [4, 5] found that the plasma flow is faster at the midplane than at the top and the asymmetry decreases towards the plasma centre, the poloidal asymmetry in [6] was particularly strong for low plasma densities and could be reversed depending on the magnetic configuration. Several suggestions have been made that could explain the observed asymmetries, such as ripple effects, viscous spreading of asymmetries from the plasma edge to the core or large scale asymmetric zonal flows in [5] or electrostatic potential variations across one flux surface in [6]. However, the origin of poloidal asymmetries in the perpendicular propagation velocity of density fluctuations remains subject of current research.

This paper reports on recent measurements at the ASDEX Upgrade tokamak (AUG), where the perpendicular propagation velocity of density fluctuations is found to be independent of the poloidal angle apart from the trivial poloidal dependence of the $E \times B$ velocity. This has been previously seen in [7] around the midplane and is now studied in a wider poloidal region. Section 2 describes the diagnostic technique, the experimental set up and one plasma discharge in detail. The analysis of the DR data and velocity profiles from four different plasma scenarios are presented in section 3. A sensitivity study investigating the impact of magnetic equilibrium, hardware alignment and density profile on the asymmetry of the velocity is presented in section 4, followed by a discussion and summary in sections 5 and 6, respectively.

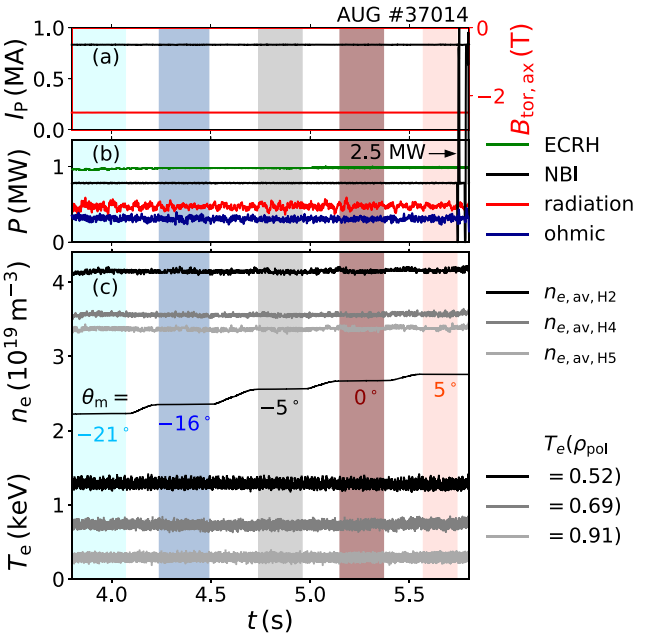

Figure 1. Plasma current and toroidal magnetic field in (a), heating and radiated power in (b) and interferometry and ECE time traces in (c) are constant during the flat top phase. The measurement intervals at different mirror angles and thus poloidal positions are shaded with colours, as well as the time trace of the mirror movement in the middle of (c).

2. Diagnostic technique and experimental set up

Doppler reflectometers [8] obliquely inject microwaves of frequency, f_0 and vacuum wavenumber, $k_0 = 2\pi f_0/c$, with the speed of light, c into the plasma at an angle, θ_0 with respect to the normal of the flux surface at the probing position. At the cutoff layer the wave is back scattered off density fluctuations with a wavenumber perpendicular to the magnetic field, $k_\perp$. In a plasma slab the back scattering process fulfils the Bragg condition, $k_\perp = 2k_0 \sin\theta_0$. In a magnetic confinement fusion device ray tracing or full-wave simulations are necessary to obtain the microwave beam trajectory.

A velocity perpendicular to the confining magnetic field, $v_\perp$ manifests itself in a Doppler shift, f_D of the backscattered signal as $v_\perp = 2\pi f_D/k_\perp$. This perpendicular velocity measured by Doppler reflectometers comprises the $E \times B$ drift velocity, $v_{E\times B}$ and the phase velocity of the turbulence, v_{ph} which depends on the probed turbulence structure size. Previous experiments performed at ASDEX Upgrade found $v_{ph} \ll v_{E\times B}$ and thus $v_\perp = v_{E\times B} + v_{ph} \approx v_{E\times B}$ [9], although this is not true for all cases [10, 11]. The finding of a much smaller phase velocity than the perpendicular propagation velocity is in line with observations within the study of this paper and has also been reported by other machines [8, 12–17]. A possible explanation is that the observed high levels of small-scale vorticity fluctuations can damp linear features such as growth rates of instabilities and thus lead to a small and dispersionless v_{ph} [18]. The $E \times B$ drift velocity yields

$$v_{E\times B} = -\frac{1}{B}\frac{\partial \Phi}{\partial r} \tag{1}$$

and depends on the local magnetic field, B and on the local gradient of the electrostatic potential, Φ. With B being proportional to the inverse major radius $1/R$, the magnetic field is not poloidally constant. Whereas the electrostatic potential is constant on each flux surface, the distance between the flux surfaces, r varies with θ_{pol}. In this paper, poloidal asymmetry other than this poloidal dependence of $v_\perp$ is not observed.

For this study $v_\perp$ is measured with a W-band Doppler reflectometer in extraordinary wave polarization (X-mode) at different poloidal locations using a steerable mirror located above the midplane on the low field side [19] of ASDEX Upgrade. ASDEX Upgrade is a medium sized tokamak with $R = 1.65$ m and minor radius $a = 0.5$ m. Dedicated experiments were carried out in low confinement mode (L-mode) deuterium plasmas. A representative discharge with a toroidal magnetic field strength B_{tor} of $B_{tor,ax} = -2.5$ T on-axis and a plasma current of $I_P = 0.8$ MA in upper single null (USN) configuration is shown in the following.

Figure 1(a) depicts time traces of the plasma current and the magnetic field for the flat top phase under consideration.

In (b) the heating power from electron cyclotron resonance heating (ECRH), neutral beam injection (NBI) and ohmic heating together with the estimated radiated power in the confined region measured by bolometery [20] is shown. The NBI blips at the end enable CXRS measurements. The top of figure 1(c) depicts the line averaged density from three interferometer signals with different lines of sight [21]. Time traces of the electron temperature at three different locations, measured by an electron cyclotron emission radiometer [22] and labelled with the poloidal magnetic flux coordinate ρ_{pol} are plotted in (c) at the bottom.

During the flat top phase the mirror of the Doppler reflectometer system is steered to different angles θ_{m}, as indicated in (c) in the middle. θ_{m} is the angle of the injected microwave with respect to the horizontal plane, counting positive angles upwards. For each mirror position the injected wave frequency is stepped in plateaus of 5 ms to obtain the radial profiles.

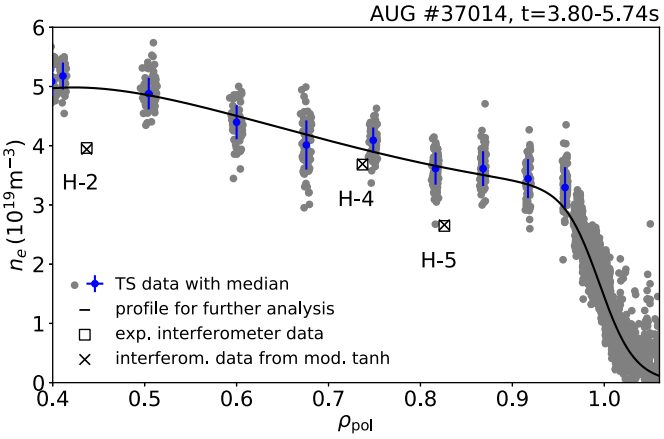

Figure 2. Density profile used for the analysis and the underlying experimental data measured with a TS diagnostic. The squares correspond to the measured interferometer values, the crosses are calculated from the density profile used for further analysis.

3. Evaluation of DR data

In order to locate the scattering position of the microwave beam in the plasma ray tracing calculations were carried out. They rely on the density profiles shown in figure 2 measured by a Thomson scattering (TS) diagnostic [23]. For the core measurements the median density and the standard deviation of the measurement data are included for all radially separated locations of measurement. The time averaged measurement values of the three interferometer lines of sight [21] are plotted at the radial position of the innermost magnetic flux surface which is intersected by the interferometer with a square symbol. The radial mapping of both TS and interferometry is done with a pressure constrained equilibrium using neo-classical current diffusion [24]. It is based on the kinetic profiles of an integrated data analysis (IDA) [25] and measurements from magnetic diagnostics. A tanh extended with a polynomial function of order 5 in the core is used as density profile for the evaluation process, details on the function can be found in [26, 27]. The crosses depict the values of virtual interferometers, where the fitted density profile is line integrated along the paths of the actual interferometers. They are in excellent agreement with the very accurate experimental interferometer data.

This density profile together with the pressure constrained equilibrium is used as input for the beam tracing code TORBEAM [28, 29], in this case neglecting relativistic effects. Figure 3(a) shows X-mode microwave beam trajectories in a poloidal cross section of ASDEX Upgrade. The different mirror angles are in blue, black and red colours and representative frequencies have different line styles. All beams come from a common launching position on the rotation axis of the mirror. A zoom in the measurement region is depicted in (b). Lines of constant cutoff frequencies are drawn in green, the poloidal magnetic flux surfaces are shown in grey and the vacuum vessel in black. The ray turning points are marked with symbols.

Outside of the plasma the refractive index is 1 and all beams of same frequency have the same wavenumber. Depending on the angle of incidence and thus the path of the trajectory the wavenumbers take different values for the same radial probing position ρ_{pol}. Figure 3(c) shows the wavenumber along the trajectories for some frequencies. Whereas for ordinary wave polarization (O-mode) all beams with similar frequency would follow the same $k_\perp$ vs. ρ_{pol} curve regardless of the injection angle and end at different wavenumbers and thus different radii, for X-mode the additional magnetic field dependence of the dispersion relation results in the different curves for different angles and frequencies. This fact will be of interest later on when the influence of the density profile on the trajectories is discussed.

The Doppler shifted peak in the frequency spectrum of the reflected microwave beam is extracted for each probing frequency using a Gaussian fit to the asymmetric part of the spectrum. Figure 4(a) depicts the measured perpendicular velocity data with the poloidal angle of the scattering volume θ_{pol} as colour scale. Negative (positive) θ_{m} correspond to lower (higher) θ_{pol}. The intrinsic poloidal variation of both E and B and thus of the $E \times B$ velocity is taken into account by mapping all data to the midplane ($\theta_{\mathrm{pol}} = 0°$) considering equation (1). The electric field is assumed to poloidally vary like the inverse distance between magnetic flux surfaces of constant Φ.

The corresponding velocities $v_{\perp,\mathrm{midplane}}$ measured at different poloidal locations match well within the uncertainties and do not indicate any poloidal asymmetry beyond the trivial poloidal variation in equation (1). The density fluctuations propagate in ion diamagnetic direction. The uncertainties indicate the radial and spectral resolution obtained by the 3-point ray tracing method. Here two beams are injected into the plasma shifting the launching point by seven times the probing wavelength above and below the original launching point as a measure of the extended microwave beam width. This method relates to the optimisation of the ellipsoidal launching mirror such that the microwave beam is focused at the probing position and consists of plane wave fronts which maximises both the spatial and the spectral resolution [30, 31]. In addition possible systematic deviations of $k_\perp$ and ρ_{pol} between ray tracing and full wave simulations such as reported in [32] have been checked. [32] reports that in general

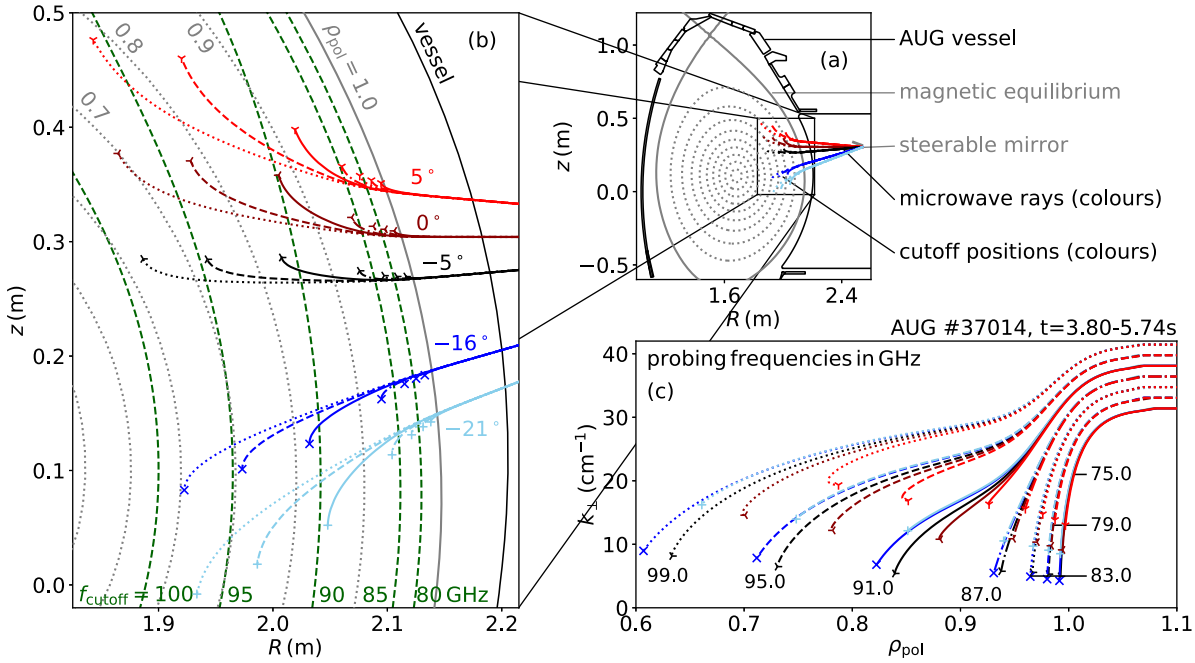

Figure 3. (a) Part of a poloidal cross section of ASDEX Upgrade and a zoom into the measurement region in (b). The cutoff frequencies for waves in X-mode polarization are dashed and the magnetic flux surfaces dotted. The trajectories of the microwaves launched in experiment are colour coded for different injection angles, have different linestyles representing the wave frequency and end at the ray turning point (symbols). (c) Turbulent wavenumbers probed along the trajectories in the plasma for different injection angles (colours) and frequencies (linestyles).

ray tracing overestimates the wavenumber at the region of maximum interaction between beam and plasma and finds the probing position at slightly smaller radii than full wave simulations. The resulting increase of $v_{\perp,\mathrm{midplane}}$ and outwards shift of all data points lie within the scatter of the data, thus having no influence on the main result of the paper. As the radial resolution depends on the launching angle, different poloidal measurement positions at the same ρ_{pol} detect contributions from radial intervals of different sizes and thus a different mix of of radially varying $v_{\perp,\mathrm{midplane}}$. However, for a velocity profile with slowly changing curvature such as in figure 4(a) this only broadens the backscattered wave spectrum but does not shift it to other frequencies. In the plasma under consideration therefore this effect does not invoke an artificial poloidal dependence of $v_{\perp,\mathrm{midplane}}$.

Towards the edge plasma the density fluctuations at the midplane move slightly faster than on the top, which is however within the uncertainties of the 3-point ray tracing method and additionally sensitive to the choice of the density profile as will be in more detail discussed in section 4.3.

Figure 4(b) shows the same velocity data colour coded with respect to the inverse turbulence scale $k_\perp$. Beams injected close to (far from) perpendicular incidence probe large (small) turbulence scales. Different turbulence scales propagate with the same velocity $v_{\perp,\mathrm{midplane}}$. As all velocity data have been mapped to the midplane taking into account the poloidal dependence of the $E\times B$ velocity, v_{ph} must either be much smaller than $v_{E\times B}$, follow the poloidal dependence of $v_{E\times B}$ within the scatter of the data or both.

The velocity profiles shown above are compared to $v_{E\times B}$ measurements on Boron from CXRS diagnostics [33, 34] close to the midplane. The radial electric field is used as defined in [35],

$$E_r = \frac{1}{n_{\mathrm{B}} Z_{\mathrm{B}} e}\frac{\partial p_{\mathrm{B}}}{\partial r} - v_{\mathrm{pol,B}} B_{\mathrm{tor}} + v_{\mathrm{tor,B}} B_{\mathrm{pol}} \qquad (2)$$

where in the core the product of toroidal velocity $v_{\mathrm{tor,B}}$ and local poloidal magnetic field B_{pol} as the dominant contribution to the radial electric field [36] is measured. The contribution of the core pressure gradient $\frac{\partial p_{\mathrm{B}}}{\partial r}$ with the prefactors n_{B} the boron density, its charge state $Z_{\mathrm{B}} = 5$ and the elementary charge e is also taken into account. The core CXRS data are shown in figure 4 as green dots. The poloidal velocity $v_{\mathrm{pol,B}}$ has not been measured in this radial region, but an analysis of several L-mode scenarios in the past showed that it stays within -1.5 to $+2$ km s^{-1} [37], which is in quantitative agreement to findings at other tokamaks [38–41]. The error bars combine measurement uncertainties of the toroidal velocity and the standard deviation of the data's scatter during the NBI blip. The edge CXRS data are shown as green line with error bars at three representative locations. They include all three terms of equation (2), whereas the larger uncertainties stem from the scatter of the poloidal velocity measurements. DR and CXRS velocity measurements agree within the error bars. Only one data point at $\rho_{\mathrm{pol}} = 0.93$ deviates by 26% which might be due to the increasing impact of the poloidal velocity towards the edge. The good agreement supports the observation of small poloidal velocities in the core and points towards $v_\perp \approx v_{E\times B}$.

In figure 5(a) the perpendicular velocity is plotted over the poloidal angle for four radial regions, which are indicated as arrows in figure 4. Following equation (1) any expected poloidal dependence from the $E\times B$ velocity is considered and

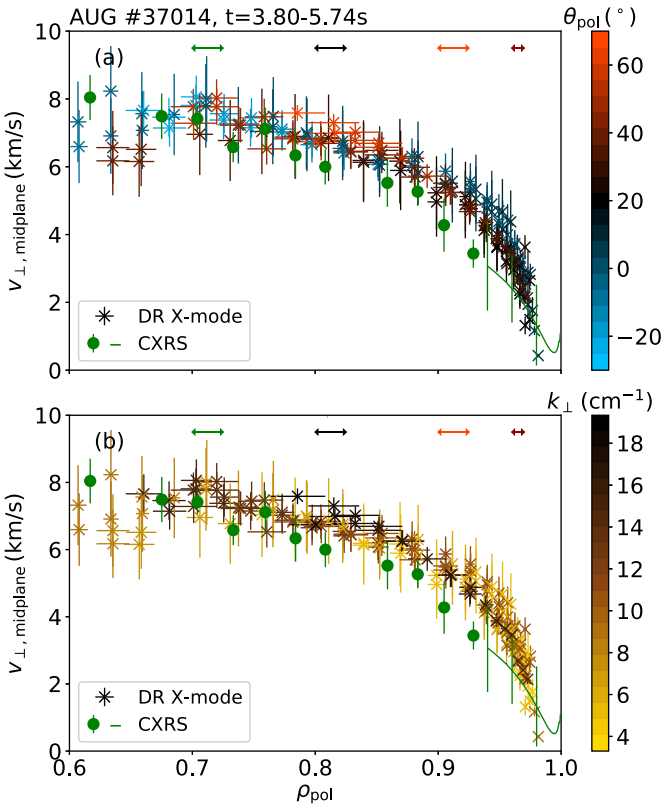

Figure 4. The perpendicular propagation velocity of density fluctuations over a large range of poloidal angles (colour coded in (a)) and inverse turbulence scales (colour coded in (b)). It matches measurements of the $E \times B$ velocity performed with CXRS where E is calculated from the toroidal velocity component and the pressure gradient term in the core and from equation (2) in the edge.

all data is mapped to the midplane, such as in figure 4. The dotted lines and the shaded areas in figure 5 correspond to the mean velocities and the standard deviation of $v_\perp$ within each radial region, respectively. Regardless of $k_\perp$ which largely varies over the poloidal angle, the perpendicular velocity is constant over the full poloidal region accessible with the current Doppler reflectometer hardware.

During extensive analyses for this paper many other L-mode plasma scenarios have been carefully evaluated of which three more are shown in figures 5(b)–(d) which are performed in the same measurement campaign as AUG #37014. Table 1 lists the most important plasma parameters of all four discharges presented in figure 5. Both magnetic configurations, USN and LSN (lower single null) are covered, such as a variety of core averaged densities $n_{\mathrm{e,av,core}}$ which are measured by an interferometer with a central line of sight.

The analysis of all discharges is identical to what was discussed in detail for discharge AUG #37014. Pressure constrained equilibria and density profiles matching both TS and interferometer measurements served as input for ray tracing done with the code TORBEAM. The Doppler shifts have been extracted from measurements with the identical in- and ex-vessel DR hardware system. All previously discussed arguments hold for these additional L-mode discharges as well.

The different heating mixes (ECRH+NBI, NBI only, ECRH only, Ohmic) lead to propagation velocities in both ion diamagnetic direction with positive sign (ECRH+NBI in (a), NBI only in (b)) and electron diamagnetic direction with negative sign (ECRH only in (d), Ohmic in (c)). For each discharge the radial windows for which $v_{\perp,\mathrm{midplane}}$ is presented in figure 5 are chosen such that $v_{\perp,\mathrm{midplane}}$ has a weak radial variation within them.

All four discharges indicate that for the measurement region accessible with the above presented hardware the perpendicular velocity does not depend on the poloidal angle within the uncertainties. A careful look into the NBI heated discharge reveals a slight dependence of $v_{\perp,\mathrm{midplane}}(\theta_{\mathrm{pol}})$ for some ρ_{pol} and θ_{pol}. This is however well within the uncertainties which arise from a variation of the electron density and are especially significant in low density cases. In summary the perpendicular velocities presented in four plasma discharges are poloidally symmetric for a careful reconstruction of the magnetic equilibrium and density profile.

4. Assessment of uncertainties of input for ray tracing

The conclusion that the perpendicular propagation velocity does not depend on the poloidal position sensitively depends on the used magnetic equilibrium, the alignment and calibration of the optics and the density profile reconstruction. If not treated with care each element can introduce errors in the ray tracing calculations and thus lead to artificial poloidal asymmetries.

This section investigates the impact of the above mentioned factors on the DR measurements and their influence on poloidal asymmetries. In the scope of this study only ray tracing effects are analysed. Possible uncertainties propagating from the determination of the Doppler shift of the microwave to $v_\perp$ are not considered as they are believed to be comparably small.

For each mirror position of the above analysed plasma discharge (as indicated in figure 3) a frequency is chosen which lies between 92 (low $k_\perp = 5.6\ \mathrm{cm}^{-1}$) and 99 GHz (high $k_\perp = 19.3\ \mathrm{cm}^{-1}$) so that the ray turning position is closest to $\rho_{\mathrm{pol}} = 0.8$. The change of the perpendicular velocity is calculated as

$$\frac{\Delta v_\perp}{v_{\perp,\mathrm{ref}}} = \frac{v_{\perp,\mathrm{new}} - v_{\perp,\mathrm{ref}}}{v_{\perp,\mathrm{ref}}} = \frac{2\pi f_{\mathrm{D}}/k_{\perp,\mathrm{new}} - 2\pi f_{\mathrm{D}}/k_{\perp,\mathrm{ref}}}{2\pi f_{\mathrm{D}}/k_{\perp,\mathrm{ref}}} = \frac{k_{\perp,\mathrm{ref}} - k_{\perp,\mathrm{new}}}{k_{\perp,\mathrm{new}}} = -\frac{\Delta k_\perp}{k_{\perp,\mathrm{new}}}. \quad (3)$$

$v_{\perp,\mathrm{ref}}$ and $k_{\perp,\mathrm{ref}}$ are the perpendicular velocity and wavenumber from section 3 obtained with the density profile in figure 2 and the pressure constrained equilibrium from [24]. $v_{\perp,\mathrm{new}}$ and $k_{\perp,\mathrm{new}}$ correspond to the ray tracing done for various optics positions, a different magnetic equilibrium or different density profiles. Strictly speaking for injection of two beams with same frequency, the assumption that f_{D} from *ref* and *new* is the same does not hold because the beams land at slightly different radial positions with potentially different

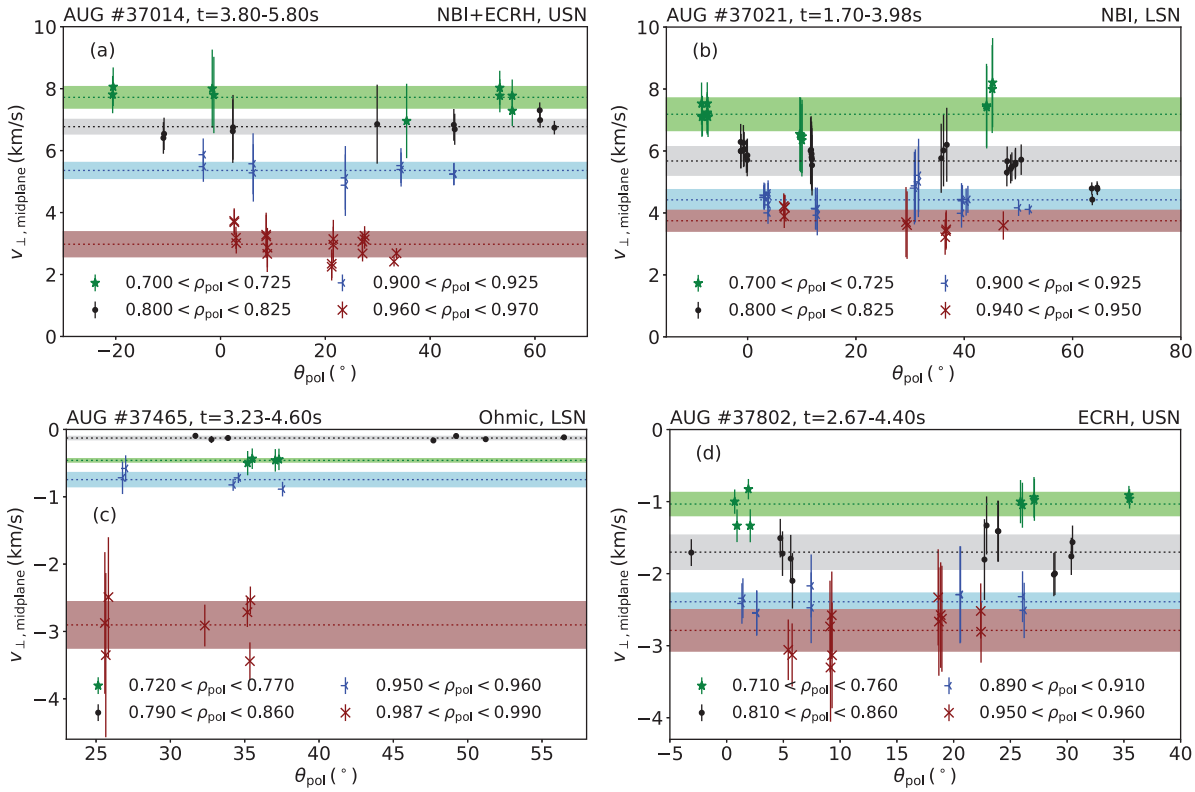

Figure 5. The perpendicular velocity of four different plasma scenarios is shown for four radial intervals and is constant over the poloidal angle.

Table 1. Key plasma parameters of the discharges presented in figure 5.

		$B_{\mathrm{tor,ax}}$ (T)	I_{P} (MA)	$n_{\mathrm{e,av,core}}$ (10^{19} m^{-3})	P_{ECRH} (MW)	P_{NBI} (MW)
37014	USN	−2.5	0.8	4.2	1.0	0.8
37021	LSN	−2.5	0.8	2.5	0.0	0.8
37465	LSN	−2.5	0.8	4.9	0.0	0.0
37802	USN	−2.5	0.9	5.2	0.7	0.0

$v_\perp$ and f_{D}. However, as shown in figure 4 the velocity profile at $\rho_{\mathrm{pol}} = 0.8$ has no strong radial gradient, and a small radial shift does not significantly change $v_\perp$, thus this simplification will be used in the following. The uncertainties in figure 6 are the same as in the perpendicular velocity profile in figure 4 at $\rho_{\mathrm{pol}} = 0.8$. For the magnetic equilibrium and hardware alignment $\Delta v_\perp / v_{\perp,\mathrm{ref}}$ slowly varies with radius up to a maximum difference of 50%. The level of radial variation of $\Delta v_\perp / v_{\perp,\mathrm{ref}}$ is comparable for the density, where in the extreme case only localised radial regions show artificial asymmetries up to a difference of 50% whereas others remain poloidally symmetric.

4.1. Magnetic equilibrium

Both shape and position of the reconstructed magnetic flux surfaces impact the ray tracing. To assess the importance of this effect, velocity profiles resulting from two different magnetic equilibria are compared: the already used pressure constrained equilibrium [24] and an equilibrium from the CLISTE code which here does not take into account measured kinetic profiles but only considers measurements from magnetic diagnostics [42, 43]. Figure 6(a) depicts the change of the perpendicular velocity. The velocities obtained for the different equilibria do not deviate strongly even though at $\rho_{\mathrm{pol}} = 0.8$ the CLISTE equilibrium is shifted radially outwards by 1.5 cm at the midplane of the low field side. Both equilibria produce poloidally symmetric profiles and are equally suited for reconstructing perpendicular velocity profiles measured with DR.

4.2. Hardware alignment

If the waveguides or the mirror system are misaligned, the beam is not injected from the radial and vertical position R_0 and z_0 with the injection angle θ_{m} but from $R_0+\Delta R$ and $z_0+\Delta z$ with $\theta_{\mathrm{m}} + \Delta\theta_{\mathrm{m}}$. Based on the pressure constrained equilibrium, figures 6(b)–(d) show how the velocity changes for mispositioning of ΔR, Δz and $\Delta\theta_{\mathrm{m}}$.

As the launching mirror is located comparably far away from the plasma and the rays are injected close to antiparallel to the direction of major radius, an inward shift of few cm

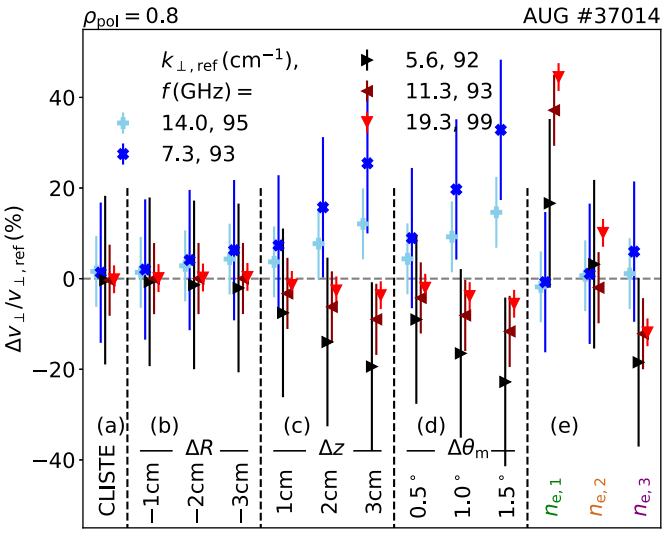

Figure 6. Relative change of the perpendicular velocity caused by various effects like the choice of the magnetic equilibrium (a), hardware misalignment in radial (b) or vertical (c) direction or with a systematic deviation in the injection angle (d) or the choice of the density profile (e). The distortion is strongest for small wavenumbers. The error bars are the same as in figure 4 at $\rho_{pol} = 0.8$.

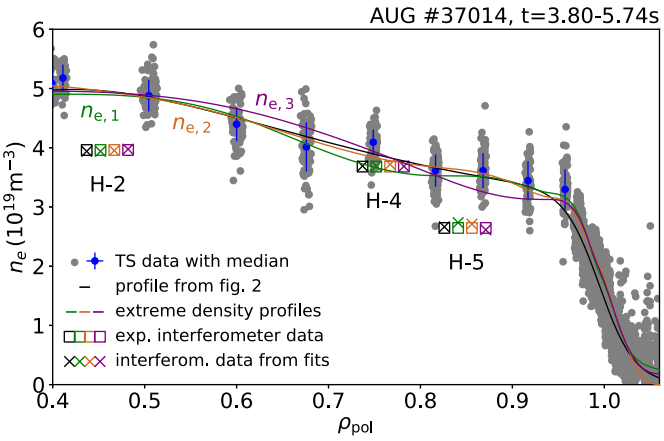

Figure 7. In colours three extreme density profiles inferred from IDA are shown which match both TS (grey and blue) and interferometry (squares) measurements. The modified tanh function used for $v_{\perp,ref}$ is depicted in black.

(negative ΔR) causes deviations from the reference velocity profile within the error bars.

More care than for the radial positioning has to be taken regarding the vertical alignment of the mirror. Already an unintended upwards shift of $\Delta z = 1$ cm leads to a clear deviation from the reference velocity which is however still within the error bars. The changes in the beam trajectory and thus $k_\perp$ are especially pronounced for small $k_\perp$ and thus small injection angles with respect to the normal of the magnetic flux surface (black and blue).

Deviations from the reference velocity profiles caused by a misalignment of the injection angle by $\Delta\theta_m$ are shown in figure 6(d). An underestimation of the injection angle of only 1° already causes asymmetries in the perpendicular velocity which are outside the error bars. Note that the velocity deviation differs in sign depending on the beam launching direction above or below perpendicular incidence (above or below $\theta_m \approx -11°$) and is again most pronounced for small injection angles where the same absolute change causes the largest relative change.

The in-vessel mirror alignment can only be checked in air and without magnetic field. The uncertainties for this measurement are 2 mm for R and z and 0.04° for θ_m which take into account the finite beam size of the optical laser used for calibration and the uncertainties of the three-dimensional measurement arm. At ASDEX Upgrade the distortion of the vessel after evacuation and baking is 0.7 mm in vertical direction and 0.7 mm in radial direction. This has been measured at the A-port of sector 9, which can, due to axissymmetry be assumed to also apply to sector 11 where the Doppler reflectometer is located.

All arguments hold for the other way around, namely a possible misplaced plasma equilibrium in horizontal or vertical direction. Note that deviations of similar relative magnitude are obtained for O-mode polarisation for different equilibria or faulty hardware alignment. Corresponding ray tracing found that O-mode results reproduce those of X-mode and is thus not shown.

To sum up, hardware misalignment, in particular errors in the launching angle, can significantly distort the measurement data and cause artificial asymmetries. The measurement uncertainty of the ASDEX Upgrade calibration technique is $\Delta\theta_m = 0.04°$ whereas figures 6(b)–(d) show that only misalignments of the order of $\Delta\theta_m = 0.5°$ leads to asymmetric velocity profiles outside the error bars.

4.3. Density profiles

The beam trajectory and $k_\perp$ directly react on the local refractive index N and its gradient ∇N which depend on the local electron density n_e and electron density gradient ∇n_e. As for X-mode N also depends on the local magnetic field B, a variation of the density profile leads to a poloidally asymmetric change of the cutoff frequency. Depending on θ_m the density change thus results in poloidally asymmetric changes of $k_\perp$ and consequently $v_\perp$. Deviations in the plasma density induce particularly strong asymmetries in low density plasmas because of the higher derivative of the cutoff frequency with respect to the density than in higher density plasmas.

To show the impact of the density profile on the poloidal dependence of DR data, three density profiles are chosen which represent cases where the absolute value and the gradient are particularly different. Figure 7 shows extreme cases calculated with the IDA analysis [25] which are not claimed to be the most likely density profiles for the time interval of consideration, but which still lie within the experimental error bars of the density diagnostics. The TS and interferometer data are depicted as in figure 2, but for the sake of visibility the coloured squares and crosses are plotted at slightly different radii. The crosses are values of virtual interferometers calculated as discussed for figure 2. The radial region with the largest impact

on the ray propagation and thus on $k_\perp$ starts at slightly larger radii than the cutoff position and ends at the cutoff position.

Figure 6(e) depicts how the choice of the density profile affects the probed wavenumber and thus can induce artificial asymmetries. The green profile $n_{e,1}$ which has a flat gradient from $\rho_{pol} = 0.85$ inwards, causes strong asymmetries at the radius under investigation, $\rho_{pol} = 0.8$. The velocity in regions above the midplane is significantly larger than the reference velocity and monotonically decreases with decreasing poloidial angle. $\Delta v_\perp / v_{\perp,ref}$ is far less pronounced for profiles such as $n_{e,2}$ where the density gradient outside and at $\rho_{pol} = 0.8$ is comparable to the gradient of the modified tanh function used for the reference velocity. Reversed asymmetries where the midplane is faster than the region above are induced by the purple density profile $n_{e,3}$. Other than for the equilibrium and hardware alignment where the artificial asymmetry has no large radial variation, the density profile can cause very local deviations from the reference velocity. Measurements far from the midplane are especially vulnerable to the density profile reconstruction than measurements close to the midplane.

In summary the choice of the density potentially causes significant asymmetries which in some cases ($n_{e,1}$) show a monotonic dependence on the poloidal angle.

5. Discussion

The absence of a poloidal dependence of the perpendicular propagation velocity of density fluctuations other than stated in equation (1) is at variance with observations from TEXTOR, Tore Supra and TJ-II where asymmetries have been found [4–6]. [4, 5] reported the strongest asymmetries in the edge comparing the midplane and the top. The question why other machines observed poloidal asymmetries, but ASDEX Upgrade did not remains open. Velocity deviations up to a factor of 4 as reported for Tore Supra are certainly outside of any conceivable error bars. The same holds for TJ-II where velocity asymmetries up to factors of 2.5 were measured and in addition significant asymmetries in the fluctuation intensity reported.

Due to hardware constraints the poloidal region covered at ASDEX Upgrade was smaller than in [4–6], in particular towards the edge. However, no trend was seen outside the uncertainties that could point towards an asymmetry for poloidally more separated regions. Additional details will be brought by a top launch reflectometer which is currently being built at ASDEX Upgrade and will enable measurements at poloidal angles of around 90°.

First investigations of ASDEX Upgrade discharges have also revealed asymmetries especially pronounced for small $k_\perp$ [44]. In the 2019 campaign the measurements had to be carried out using a launching mirror optimised for monostatic operation but operated in bistatic. Thus the overlap of the emitting and receiving ray at the cutoff was only possible via a non-zero parallel component of the wavevector. This might have additionally shifted the measurement position in poloidal direction, imposing a deviation especially strong for small $k_\perp$ and the plasma core.

The uncertainties obtained by the 3-ray method strongly depend on $k_\perp$ and are largest for small wavenumbers. This reflects that ray tracing for small $k_\perp$ is most vulnerable to artificially induced asymmetries. The error bars in figures 4 and 6 give an optimistic lower limit for the asymmetries resolvable by DR. Whereas misalignment of hardware gives systematic asymmetries, the choice of the equilibrium and the density profile potentially causes asymmetries which vary on a shot to shot basis.

6. Summary and conclusion

This paper reports on the absence of poloidal velocity asymmetries in the ASDEX Upgrade tokamak. The perpendicular velocity of density fluctuation is found to only follow the poloidal dependence of the $E \times B$ drift velocity. Furthermore the perpendicular velocity of several turbulence structure sizes is found to be the same. The analysis of one discharge has been in detail presented. It is representative for a large amount of low confinement discharges under various conditions. Three more plasma scenarios have been shown with different heating mixes of beam and microwave heating in a wide range of plasma densities in both lower and USN magnetic configuration. Within the measurement region accessible by the current diagnostic hardware, no poloidal asymmetry other than the $E \times B$ dependence was found.

A detailed explanation of ray tracing is followed by a sensitivity study of how analysis uncertainties in input for ray tracing may induce artificial asymmetries. Both hardware misalignments and incorrect magnetic equilibrium or density profile reconstruction potentially introduce asymmetries outside the error bars. Artificial asymmetries are especially pronounced for misalignments in the injection angle close to perpendicular incidence and are highly sensitive to the density profile. Whereas the velocity deviations caused by the first are systematic and observable over all radial regions, they are more localised and potentially different on a shot to shot basis for the latter.

Acknowledgments

We express special thanks to J Friesen for his excellent hardware support and acknowledge G D Conway for useful discussions. This work has been carried out within the framework of the EUROfusion Consortium and has received funding from the Euratom research and training programme 2014–2018 and 2019–2020 under Grant Agreement No. 633053. The views and opinions expressed herein do not necessarily reflect those of the European Commission.

ORCID iDs

K Höfler https://orcid.org/0000-0001-7925-8159
T Happel https://orcid.org/0000-0003-4364-9363
P Hennequin https://orcid.org/0000-0002-4848-4898
R M McDermott https://orcid.org/0000-0002-8958-8714

References

[1] Wootton A J *et al* 1990 Fluctuations and anomalous transport in tokamaks *Phys. Fluids* B **2** 2879–903

[2] Liewer P C 1985 Measurements of microturbulence in tokamaks and comparisons with theories of turbulence and anomalous transport *Nucl. Fusion* **25** 543

[3] Biglari H *et al* 1990 Influence of sheared poloidal rotation on edge turbulence *Phys. Fluids* B **2** 1–4

[4] Krämer-Flecken A *et al* 2012 Poloidal rotation asymmetry and relation to turbulence *39th EPS Conf. and 16th Int. Congress on Plasma Physics 2–6 July 2012 Stockholm, Sweden* vol 36F (Mulhouse: European Physical Society) (http://ocs.ciemat.es/epsicpp2012pap/pdf/P5.044.pdf)

[5] Vermare L *et al* 2018 Poloidal asymmetries of flows in the Tore Supra tokamak *Phys. Plasmas* **25** 020704

[6] Estrada T *et al* 2019 Turbulence and perpendicular plasma flow asymmetries measured at TJ-II plasmas *Nucl. Fusion* **59** 076021

[7] Lechte C *et al* 2017 X mode Doppler reflectometry k-spectral measurements in ASDEX Upgrade: experiments and simulations *Plasma Phys. Control. Fusion* **59** 075006

[8] Hirsch M *et al* 2001 Doppler reflectometry for the investigation of propagating density perturbations *Plasma Phys. Control. Fusion* **43** 1641

[9] Viezzer E *et al* 2013 High-accuracy characterization of the edge radial electric field at ASDEX Upgrade *Nucl. Fusion* **53** 053005

[10] Conway G D *et al* 2006 Observations on core turbulence transitions in ASDEX Upgrade using Doppler reflectometry *Nucl. Fusion* **46** S799

[11] Happel T *et al* 2015 Core turbulence behavior moving from ion-temperature-gradient regime towards trapped-electron-mode regime in the ASDEX Upgrade tokamak and comparison with gyrokinetic simulation *Phys. Plasmas* **22** 032503

[12] McKee G *et al* 2000 Impurity-induced suppression of core turbulence and transport in the DIII-D tokamak *Phys. Rev. Lett.* **84** 1922

[13] Hirsch M *et al* 2006 Dynamics of poloidal flows and turbulence at the H-mode transition in W7-AS *Plasma Phys. Control. Fusion* **48** S155

[14] Hennequin P *et al* 2005 Doppler backscattering on Tore Supra: perpendicular velocity profile and k-spectrum in high ICRH experiments *7th Int. Reflectometry Workshopfor Fusion Plasma Diagnostics (IRW7) 9–12 May 2005 Garching, Germany* (Garching: Max-Planck-Institut für Plasmaphysik) 74 (www.aug.ipp.mpg.de/IRW/IRW7/papers/Hennequin-paper.pdf)

[15] Hennequin P *et al* 2006 Fluctuation spectra and velocity profile from Doppler backscattering on Tore Supra *Nucl. Fusion* **46** S771

[16] Trier E *et al* 2008 Radial electric field measurement in a tokamak with magnetic field ripple *Nucl. Fusion* **48** 092001

[17] Estrada T *et al* 2009 Sheared flows and transition to improved confinement regime in the TJ-II stellarator *Plasma Phys. Control. Fusion* **51** 124015

[18] Manz P *et al* 2018 On the phase velocity in between weak and strong plasma edge turbulence *Plasma Phys. Control. Fusion* **60** 085002

[19] Happel T *et al* 2011 Design of a new Doppler reflectometer frontend for the ASDEX Upgrade tokamak *10th Int. Reflectometry Workshop for Fusion Plasma Diagnostics (IRW10) 4–6 May 2011 Padova, Italy* (Garching: Max-Planck-Institut für Plasmaphysik) 1007 (www.aug.ipp.mpg.de/IRW/IRW10/papers/1007-IRW10-HappelT-paper.pdf)

[20] Bernert M 2013 Analysis of the H-mode density limit in the ASDEX Upgrade tokamak using bolometry *PhD Thesis* (Ludwig-Maximilians-Universität München) (https://doi.org/10.5282/edoc.16262)

[21] Mlynek A *et al* 2010 Design of a digital multiradian phase detector and its application in fusion plasma interferometry *Rev. Sci. Instrum.* **81** 033507

[22] Denk S S *et al* 2018 Analysis of electron cyclotron emission with extended electron cyclotron forward modeling *Plasma Phys. Control. Fusion* **60** 105010

[23] Murmann H *et al* 1992 The Thomson scattering systems of the ASDEX Upgrade tokamak *Rev. Sci. Instrum.* **63** 4941

[24] Fischer R *et al* 2013 Magnetic equilibrium reconstruction using geometric information from temperature measurements at ASDEX Upgrade *40th EPS Conf. on Plasma Physics 1–5 July 2013 Espoo, Finland* vol 37D (http://ocs.ciemat.es/EPS2013PAP/pdf/P2.139.pdf)

[25] Fischer R *et al* 2010 Integrated data analysis of profile diagnostics at ASDEX Upgrade *Fusion Sci. Technol.* **58** 675

[26] Groebner R J *et al* 1998 Scaling studies of the high mode pedestal *Phys. Plasmas* **5** 1800–6

[27] Schneider P A 2012 Characterization and scaling of the tokamak edge transport barrier *Dissertation* (Ludwig–Maximilians–Universität München) (https://doi.org/10.5282/edoc.14723)

[28] Poli E *et al* 2001 TORBEAM, a beam tracing code for electron-cyclotron waves in tokamak plasmas *Comput. Phys. Commun.* **136** 90–104

[29] Poli E *et al* 2018 TORBEAM 2.0, a paraxial beam tracing code for electron-cyclotron beams in fusion plasmas for extended physics applications *Comput. Phys. Commun.* **225** 36–46

[30] Hirsch M *et al* 2004 Doppler reflectometry with optimized temporal resolution for the measurement of turbulence and its propagation velocity *Plasma Phys. Control. Fusion* **46** 593

[31] Bulanin V V *et al* 2006 Spatial and spectral resolution of the plasma Doppler reflectometry *Plasma Phys. Rep.* **32** 47–55

[32] Conway G D *et al* 2019 Recent progress in modelling the resolution and localization of Doppler reflectometry measurements *14th Int. Reflectometry Workshop for Fusion Plasma Diagnostics (IRW14) 22–24 May 2019 Lausanne, Switzerland* (Garching: Max-Planck-Institut für Plasmaphysik) p O.213 (www.aug.ipp.mpg.de/IRW/IRW14/papers/213-IRW14-Conway-paper.pdf)

[33] Viezzer E *et al* 2012 High-resolution charge exchange measurements at ASDEX Upgrade *Rev. Sci. Instrum.* **83** 103501

[34] Cavedon M *et al* 2017 A fast edge charge exchange recombination spectroscopy system at the ASDEX Upgrade tokamak *Rev. Sci. Instrum.* **88** 043103

[35] Viezzer E 2012 Radial electric field studies in the plasma edge of ASDEX Upgrade *PhD Thesis* (Ludwig-Maximilians-Universität München) (https://doi.org/10.5282/edoc.16157)

[36] Lebschy A *et al* 2015 Indirect measurement of the poloidal rotation in the core of ASDEX Upgrade plasmas with charge exchange recombination spectroscopy *42nd EPS Conf. on Plasma Physics 22–26 June 2015 Lisbon, Portugal* vol 39E (Mulhouse: European Physical Society) (http://ocs.ciemat.es/EPS2015PAP/pdf/P1.137.pdf)

[37] Lebschy A 2018 Experimental characterization of the core plasma flow at the ASDEX Upgrade tokamak *PhD Thesis* (Technische Universität München) (https://mediatum.ub.tum.de/1428276)

[38] Brau K *et al* 1983 Plasma rotation in the PDX tokamak *Nucl. Fusion* **23** 1643

[39] Bell R E *et al* 2010 Comparison of poloidal velocity measurements to neoclassical theory on the National Spherical Torus Experiment *Phys. Plasmas* **17** 082507

[40] Chrystal C *et al* 2012 Calculation of impurity poloidal rotation from measured poloidal asymmetries in the toroidal rotation of a tokamak plasma *Rev. Sci. Instrum.* **83** 10D501
[41] Bortolon A *et al* 2013 Indirect measurement of poloidal rotation using inboard–outboard asymmetry of toroidal rotation and comparison with neoclassical predictions *Nucl. Fusion* **53** 023002
[42] McCarthy P J, Martin P and Schneider W 1999 The CLISTE Interpretative Equilibrium Code *Technical Report IPP 5/85* (Garching: Max-Planck-Institut für Plasmaphysik) (www.edoc.mpg.de/413804)
[43] Schneider W *et al* 2000 ASDEX Upgrade MHD equilibria reconstruction on distributed workstations *Fusion Eng. Des.* **48** 127–34
[44] Höfler K *et al* 2019 Study of poloidal asymmetries in the flow velocity perpendicular to the magnetic field of the ASDEX Upgrade tokamak *14th Int. Reflectometry Workshop for Fusion Plasma Diagnostics (IRW14) 22–24 May 2019 Lausanne, Switzerland* (Garching: Max-Planck-Institut für Plasmaphysik) p O.304 (www.aug.ipp.mpg.de/IRW/IRW14/papers/304-IRW14-Hoefler-paper.pdf)